



# Groundwater flow and its effect on salt dissolution in Gypsum Canyon watershed, Paradox Basin, southeast Utah, USA

Nadine G. Reitman · Shemin Ge · Karl Mueller

**Abstract** Groundwater flow is an important control on subsurface evaporite (salt) dissolution. Salt dissolution can drive faulting and associated subsidence on the land surface and increase salinity in groundwater. This study aims to understand the groundwater flow system of Gypsum Canyon watershed in the Paradox Basin, Utah, USA, and whether or not groundwater-driven dissolution affects surface deformation. The work characterizes the groundwater flow and solute transport systems of the watershed using a three-dimensional (3D) finite element flow and transport model, SUTRA. Spring samples were analyzed for stable isotopes of water and total dissolved solids. Spring water and hydraulic conductivity data provide constraints for model parameters. Model results indicate that regional groundwater flow is to the northwest towards the Colorado River, and shallow flow systems are influenced by topography. The low permeability obtained from laboratory tests is inconsistent with field observed discharges, supporting the notion that fracture permeability plays a significant role in controlling groundwater flow. Model output implies that groundwater-driven dissolution is small on average, and cannot account for volume changes in the evaporite deposits that could cause surface deformation, but it is speculated that dissolution may be highly localized and/or weaken evaporite deposits, and could lead to surface deformation over time.

**Keywords** Groundwater flow · Solute transport · Dissolution · Numerical modeling · USA

## Introduction

Groundwater is a primary control on dissolution of subsurface evaporite (salt) deposits. Subsurface salt flow and dissolution can drive extensional faulting and associated subsidence on the land surface, increased salinity in groundwater, and salt input to river systems (Benito et al. 1998, 2000; Guerrero et al. 2004; Gutiérrez 2004). Previous studies have investigated long-term structural deformation as a result of salt dissolution (Ge and Jackson 1998; Walsh and Schultz-Ela 2003), density-driven groundwater flow near salt structures (Evans et al. 1991; Ranganathan and Hanor 1988), and dissolution as a geologic hazard (Johnson 2005), but few studies have been conducted to constrain watershed-scale dissolution over short time periods.

In the Paradox Basin, a northwest–southeast trending asymmetric basin in southwest Colorado and southeast Utah, USA, evidence for growth and deformation of salt structures is abundant (Furuya et al. 2007; Jackson et al. 1998; McCleary and Romie 1986; Trudgill 2002; Walsh and Schultz-Ela 2003), but dissolution has been neither quantified nor investigated on decadal or shorter time scales. The Paradox Basin is approximately 190 km wide by 265 km long (Barbeau 2003) and is comprised of regional sedimentary formations underlain by Paradox Formation evaporite deposits. It is defined by the maximum extent of evaporite salt cycles of the Paradox Formation (Condon 1997; Nuccio and Condon 1996) and now sits in the central Colorado Plateau, cut by the Colorado River.

Gypsum Canyon watershed (38°N, 110°W; Fig. 1), in the midwestern portion of the Paradox Basin, was selected for study due to its location near actively deforming faults (Fig. 1) and the presence of groundwater springs within it. The watershed is bounded by the Colorado River in the northwest, the Needles District of Canyonlands National Park in the north, and the Abajo Mountains in the southeast. Gypsum Canyon watershed is ~310 km<sup>2</sup> with its longest dimension, ~28 km, on the diagonal. Active faults adjacent to the study area, including Imperial Valley Fault (Fig. 1) on the border of the studied watershed, slip at a rate of approximately 1–2 mm/year (Furuya et al. 2007), possibly due to salt dissolution. It is suspected that groundwater plays a role in salt dissolution and surface deformation, yet little is known about the groundwater

Received: 1 May 2013 / Accepted: 23 February 2014  
Published online: 17 April 2014

© Springer-Verlag Berlin Heidelberg 2014

N. G. Reitman (✉) · S. Ge · K. Mueller  
Department of Geological Sciences,  
University of Colorado - Boulder, UCB 399,  
2200 Colorado Ave, Boulder, CO 80309-0399, USA  
e-mail: nadine.reitman@colorado.edu

*Present Address:*

N. G. Reitman  
Geologic Hazards Science Center, U.S. Geological Survey,  
1711 Illinois St, Golden, CO 80401, USA

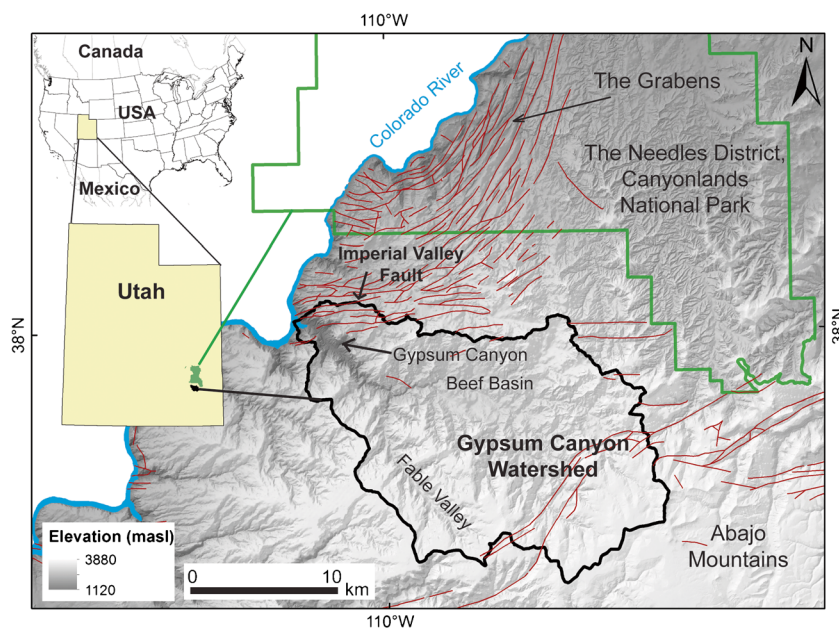


**Fig. 1** Map of Gypsum Canyon watershed in a regional context. Location of the studied watershed is *outlined in black*. Faults are *red*. The Needles District is the area east of the Colorado River within the Canyonlands National Park boundary (*green*). Elevation is in meters above sea level (masl)

system in Gypsum Canyon watershed. Better understanding of the groundwater system is thus critical for determining groundwater's role in dissolution and surface deformation.

Prior research near Canyonlands National Park has focused on groundwater as a potable water source (Bishop 1996; Cudlip et al. 1999; Martin 2001; Richter 1980; Sumison and Bolke 1972) and salt structures as depositories for nuclear waste (McCleary 1989; McCleary and Romie 1986). This study aims to provide a first-order estimate of the groundwater flow regime and solute transport dynamics in Gypsum Canyon watershed in order to assess whether these processes affect surface deformation. This report first describes the background information on the study site, then explains the collection and analysis of field data, followed by a presentation of the numerical modeling of groundwater and solute transport, and finally a discussion of the implications of the study and concluding remarks.

## Study site background

### Geology

Strata exposed in the study region (Fig. 2) range from Triassic to Pennsylvanian sedimentary units underlain by the Pennsylvanian Paradox Formation. Gypsum Canyon watershed is dominated by exposed bedrock with deep canyons, high mesas, and sediment-filled basins and washes, the result of erosion and weathering in tributaries to the Colorado River. The sedimentary units are nearly horizontal, with a regional dip of 1–2° to the northwest except for localized areas of folding and faulting, likely due to both salt

dissolution and older deformation (Baars 2010; Huntoon 1979; Walsh and Schultz-Ela 2003). McCleary and Romie (1986) speculate that Beef Basin (Fig. 1) within Gypsum Canyon watershed formed as a result of dissolution of underlying salt.

The oldest unit, the Pennsylvanian Paradox Formation is composed of shale and 29 evaporite cycles and is exposed on the floor of Gypsum Canyon near the Colorado River (Baars 2010; Condon 1997; Huntoon et al. 1982; Lewis et al. 2011; Massoth and Tripp 2011; McCleary and Romie 1986), although this could not be confirmed during fieldwork. The evaporite cycles of the Paradox Formation are primarily halite, but may also contain anhydrite and other salts (Nuccio and Condon 1996). The exact extent of the Paradox Formation evaporite cycles underlying the study area is unknown. The most recent study of the extent of Paradox Formation salts was conducted by Condon (1997) and used geophysical borehole data and computer interpolation to estimate the maximum extent of the salt deposits. Condon shows a salt pinch-out in the vicinity of Gypsum Canyon; however, there is no borehole data within the depicted pinch-out, and all boreholes surrounding the pinch-out contain salt. Therefore, for the purpose of this study it is assumed that the Paradox Formation salt deposits underlie the entire watershed.

The Pennsylvanian Honaker Trail Formation overlies the Paradox Formation and is comprised of thick limestone beds with some interbedded siltstone, fine sandstone, and shale. The Pennsylvanian–Permian lower Cutler Group beds outcrop in washes and at lower elevations and are recognized in the field by alternating layers of gray limestone, red fine sandstone, and tan coarse sandstone. The lower Cutler Group beds provide

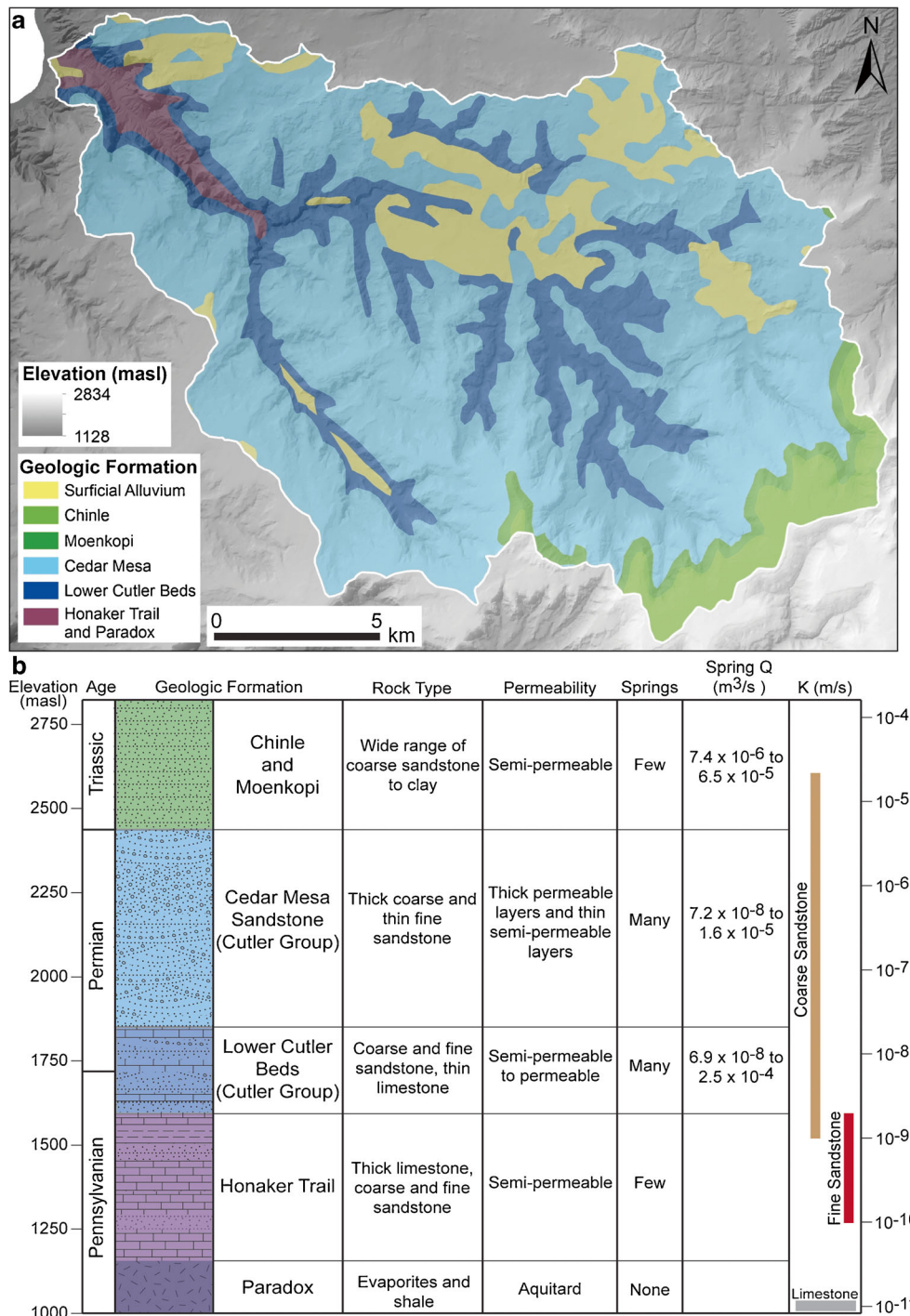


**Fig. 2** a Surface geology of Gypsum Canyon watershed. The Paradox Formation may be exposed in the bottom of Gypsum Canyon, but it is neither mapped nor accessible in the field. b Hydrostratigraphic column detailing hydrologic properties of the geologic units present in the study area. Colors correspond to legend (a). Hydraulic conductivity is shown for rock types rather than formations

the transition zone between the Honaker Trail Formation and the Cedar Mesa Sandstone, the thickest and most extensive unit in the study area. The Permian Cedar Mesa Sandstone, a member of the Cutler Group, outcrops over approximately 80 % of the study area and can be 800 m thick (Huntoon et al. 1982; Lewis et al. 2011). It is composed of thickly bedded (meter scales) tan, coarse-

grained sandstone that is often cross-bedded and thinly bedded (centimeter scales) red fine-grained sandstone.

The Triassic Chinle and Moenkopi Formations exist only in the southeast part of the study area above ~2,450 meters above sea level (masl) and consist of shale, siltstone, and sandstone and tend to form cliffs (Lewis et al. 2011). Thin surficial deposits of discontinuous

unconsolidated Quaternary alluvium and eolian deposits are exposed throughout the study area in washes and in Beef Basin.

### Climate

Climate in the study region is predominantly semi-arid to arid. No meteorological stations exist within the studied watershed, so climate data are derived from regional data and climate models. The watershed ranges in elevation from 1,128 masl at the Colorado River to 2,834 masl in the Abajo Mountains and receives 13–65 cm of precipitation per year (Fig. 3; Lugo et al. 1999; PRISM Climate Group at Oregon State University 2013; Woods et al. 1997). The highest part of the watershed, mostly above ~2,400 masl, is deciduous and coniferous forest and can receive greater than 50 cm/year of precipitation (PRISM Climate Group at Oregon State University 2013). The middle part of the watershed, the area between about 1,500–2,450 masl, is predominately semiarid benchlands and canyonlands covered with desert brush such as piñon pine and juniper trees. The lowest part of the watershed, the area below 1,500 masl, is arid desert canyonlands and usually receives less than 20 cm/year of precipitation (PRISM Climate Group at Oregon State University 2013), mostly as rain in the late summer (Woods et al. 1997). Mean annual temperatures range from approximately 6–12 °C (Lugo et al. 1999), and evapotranspiration can exceed 100 cm/year at low elevations (Richter 1980; Sumison and Bolke 1972).

### Hydrology

It is hypothesized that groundwater in the greater Canyonlands National Park region is recharged in the Abajo Mountains and through areas of high fracture density and flows predominantly northwest, towards the

Colorado River (Bishop 1996; Nuckolls and McCulley 1987; Paiz and Thackston 1987a; Richter 1980; Sumison and Bolke 1972). Aquifers in the greater region are highly heterogeneous and anisotropic due to fracture permeability, especially in the vertical direction (Richter 1980), and cyclical rock layers of varying permeability. In the greater region, most aquifers are under confined or semi-confined conditions, and perched water tables may occur locally (Bishop 1996).

Previous studies have characterized the regional geologic units in the greater Canyonlands National Park area by hydrologic properties, breaking them into hydrogeologic units with similar hydraulic conductivities (Fig. 2). According to Richter (1980) and Bishop (1996), the youngest formations, Chinle and Moenkopi, are leaky confining layers with low hydraulic conductivity except where fracture permeability dominates. The Cedar Mesa Sandstone forms the primary aquifer, with one reported hydraulic conductivity on the order of  $10^{-7}$  m/s (Bishop 1996), and the lower Cutler Group beds and the Honaker Trail Formation have more and less permeable intervals. Regionally, the Honaker Trail Formation is considered mostly an aquitard; however, it is likely that fracture permeability exists due to the presence of springs within it. The Paradox Formation has the lowest permeability of the units in the region. Evaporites and shales of the Paradox are considered an aquitard and overall flow is thought to be very slow (Paiz and Thackston 1987a).

Springs are common throughout the greater Canyonlands area in Cutler Group outcrops (Bishop 1996; Richter 1980) with fewer springs existing in the Honaker Trail and Chinle formations. Richter (1980) documented spring discharge ranging from  $6.3 \times 10^{-6}$  to  $8.2 \times 10^{-4}$  m<sup>3</sup>/s in four Cutler Group outcrop springs, and Bishop (1996) reported that one spring in the Honaker Trail Formation flows at a rate of  $2.84 \times 10^{-2}$  m<sup>3</sup>/s.

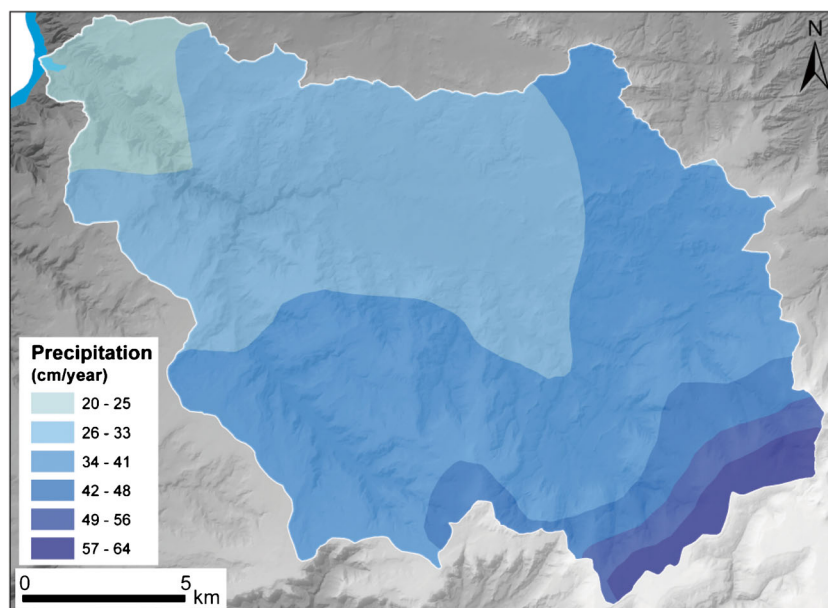


Fig. 3 Annual precipitation in Gypsum Canyon watershed. Data are estimated from PRISM (PRISM Climate Group at Oregon State University 2013)

Regionally, water quality is highly variable, and deteriorates with depth. One well drilled deeper than 25 m in the Needles District of Canyonlands National Park, north of the study area, encountered saline water (Martin 2001). A study conducted by Nuckolls and McCulley (1987) sampled nine springs discharging from the Honaker Trail Formation in the Colorado River canyon north of Gypsum Canyon watershed. They reported TDS concentrations ranging from 834 to 13,558 mg/L with the salinity originating from salt dissolution. They also found that spring water was mostly meteoric water with a small component of saline groundwater (Nuckolls and McCulley 1987).

Prior groundwater data is sparse in Gypsum Canyon watershed, but springs and seeps are common (Fig. 4). No wells exist within the studied watershed. Recharge in the study area probably occurs mostly in the southeast portion of the watershed, where elevations are above 2,100 masl and there is more precipitation. Evapotranspiration is so high at low elevations that it is unlikely that much recharge occurs; however, isotopic evidence from this study suggests that localized recharge at low elevations is possible. Discharge occurs at springs, seeps, saturated washes, and at the mouth of Gypsum Canyon into Colorado River. The springs and seeps in the study area are either contact springs, formed by water discharging from horizontal rock layers at the contact between high permeability and low permeability units, or depression springs, formed where the water table intersects the ground surface at a topographic low, as defined by Bryan (1919) and adopted by Fetter (2001). Contact springs usually drip from between bedding planes, and they occur mostly at high topographic gradients such as canyon heads, and occasionally at non-canyon locations. Depression springs occur in saturated washes or other

topographic lows. Some springs have been “extended” by inserting a PVC pipe near the spring directing water to a trough via gravity flow. Extended springs are often more reliable water sources than other springs. All seeps and springs are henceforth called “springs”. Surface water in Gypsum Canyon watershed drains into the Colorado River via its tributaries. Most streams and some springs are ephemeral.

## Field data collection and analysis

The remote location of Gypsum Canyon watershed and the lack of meteorological stations, stream gauges, or water wells within it contribute to a lack of prior data and present challenges for collecting new data. Fieldwork was conducted in May–June 2012 in order to gather data to constrain and calibrate the numerical model. Fieldwork focused on locating and sampling groundwater springs. Some springs were identified beforehand from maps (Paiz and Thackston 1987b; Richter 1980). Rock samples were also collected.

## Water sampling, rock sampling, and fieldwork

Water samples were collected from 22 groundwater springs (Fig. 4, Table 1) in plastic leak-proof 125-ml bottles and sealed with Parafilm to prevent evaporation. Water samples were only collected at naturally occurring springs. Water was sampled at extended springs directly from the pipe outlet. Depression springs were sampled by digging a small hole, about 15 cm deep or until the water table was reached, in order to access water that had not been exposed on the surface. Contact springs were sampled where they drip from between bedding planes.

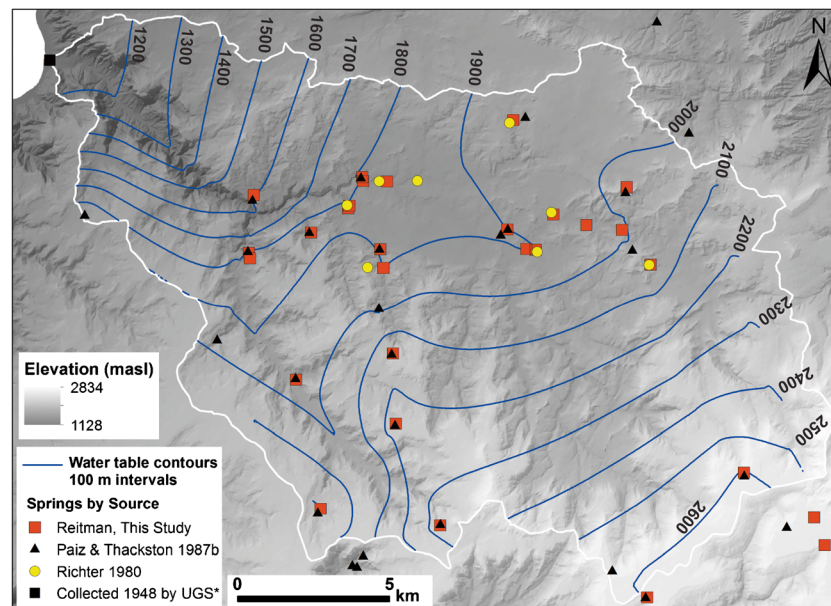


**Fig. 4** Map showing spring locations and water table contours (masl). The water table map was made using spring data and hydrologic features recorded in the field. Water flows generally from southeast to northwest, towards the Colorado River. Utah Geological Survey (UGS) 1948 spring data accessed via Utah Geological Survey (2012)

Fifteen contact springs were identified, but only nine were accessible for sampling. Plunge-pools, bleaching, cottonwood trees, and animal tracks were common features at springs, and were recorded as evidence of a shallow groundwater table or ephemeral spring, even if the area was dry during fieldwork.

Spring discharge rates were estimated in the field when possible by recording the time it took to fill a 125-ml bottle. Three sampled springs discharge from the Chinle Formation, the rest discharge from the Cutler Group. Of the approximately 30 documented springs in the watershed, 22 of them were able to be sampled, and discharge was estimated for 13 of them. Six of the discharge estimates are accurate, four are underestimates of springs with large discharge, and three are minimal underestimates of springs with small discharge. Estimated discharge is presented in Table 1. The sum of estimated discharge is  $6.6 \times 10^{-4} \text{ m}^3/\text{s}$ , but this underestimates total discharge in the watershed since discharge occurs in many unmapped locations and at the Colorado River. Of the eight springs that could not be sampled, at least four have large discharges and were inaccessible due to being in the middle of a cliff.

A total of 15 rock samples of the three most common rock types (tan coarse sandstone, red fine sandstone, and limestone) were collected throughout the watershed, from the Chinle Formation, Cedar Mesa Sandstone, and lower Cutler Group beds. Sampling bias exists for the red fine sandstone and the limestone. It was difficult to find samples of red fine sandstone with bedding thick enough to withstand permeameter tests, so samples have thicker bedding than is typical. Limestone samples were selected for their lack of fractures, not always successfully.

### Water table

Locations of groundwater springs give the best available means to estimate the location of the water table within Gypsum Canyon watershed because no water wells exist. Each hydrologic feature is a place where the height of the water table intersects with the land surface, providing a bound on the height of the water table. Point location and elevation data of springs and hydrologic features were imported into ArcGIS and interpolated using the natural neighbor method to create a water table map (Fig. 4). Hydrologic features used as point data inputs include springs, seeps, saturated topographic depressions, small streams, and vegetation suggestive of a dependable water supply. Springs recorded by Paiz and Thackston (1987b), Richter (1980), and the Utah Geological Survey (UGS) in 1948 (Utah Geological Survey 2012) that were not visited in 2012 are also included in the dataset for creating the water-table map.

The resulting water-table map follows the general pattern of topography, with higher hydraulic head in the mountains to the southeast and lower head at the Colorado River in the northwest (Fig. 4). This water table configuration suggests a general southeast–northwest pattern of groundwater flow consistent with a previous study (Bishop 1996) that reported the water table in the

Needles District, to the north of the study area, dips towards the Colorado River to the northwest.

### Stable isotope analysis

Stable isotope ratios of oxygen ( $^{18}\text{O}/^{16}\text{O}$ ) and deuterium ( $^2\text{H}/^1\text{H}$ ) in  $\text{H}_2\text{O}$  change in standard patterns, called fractionations, throughout the global hydrologic cycle (Dansgaard 1964; Bowen 2003). Fractionations occur when water molecules undergo phase changes such as evaporation and condensation. Vapor phases preferentially incorporate lighter isotopes and liquid phases preferentially incorporate heavier isotopes. The isotopic ratio of precipitation depends on the path the cloud takes between formation over the equatorial ocean and precipitating on land. Stable isotope ratios of precipitation are thus predictable around the world and vary with respect to altitude, latitude, temperature, distance from the ocean, and amount of precipitation (Dansgaard 1964). Globally, stable isotope ratios of precipitation plot on the global meteoric water line (GMWL), defined by the relationship  $\delta^2\text{H} = 8\delta^{18}\text{O} + 10$  (Craig 1961; Dansgaard 1964). Diversions from the GMWL are an indication of other processes affecting the value of the stable isotope ratio.

The stable isotopic ratio of water in an aquifer depends on the sources of water in the aquifer. Recharge will have an isotopic signature similar to precipitation, but deeper water within an aquifer may have a different isotopic signature depending on where and when it originated. Usually, once water has infiltrated an aquifer, its stable isotopic ratio is only altered by mixing with water containing a different isotopic signature. Stable isotope ratios were measured in spring water samples to better constrain the flow paths and origin of water in the springs.

Oxygen and deuterium isotopic ratios were measured for 22 spring samples. Samples were analyzed on a Picarro Cavity Ringdown Spectrometer i1102 for water isotopes. Isotope ratios are expressed as a delta ( $\delta$ ) value where  $\delta$  is equal to the difference between the sample and a standard in parts per mil (‰).  $\delta$  values are calculated using the equation:

$$\delta^{18}\text{O} = \left[ \frac{(^{18}\text{O}/^{16}\text{O})_{\text{sample}}}{(^{18}\text{O}/^{16}\text{O})_{\text{standard}}} \right] \times 1000 \quad (1)$$

The samples were compared to in-house standards calibrated to the Vienna Standard Mean Ocean Water 2 (VSMOW2) international measurement standard with an assigned reference  $\delta$  value of 0.0 ‰. Precision is 0.1 ‰ for  $\delta^{18}\text{O}$  and 1.0 ‰ for  $\delta^2\text{H}$ .

As shown in Fig. 5 and Table 1, the range of  $\delta^{18}\text{O}$  values for the samples is  $-14.9$  to  $-10.7$  ‰ (Fig. 5a). The range of  $\delta^2\text{H}$  values is  $-108$  to  $-78$  ‰ (Fig. 5b). The equation of the line formed by the measured values is  $\delta^2\text{H} = 7.16\delta^{18}\text{O} - 4.10$  (Fig. 5c). Both  $\delta^{18}\text{O}$  and  $\delta^2\text{H}$  show a weak correlation with elevation. Low-elevation springs have heavier isotopic ratios than high-elevation springs with  $R^2 = 0.72$  for  $\delta^{18}\text{O}$  and  $R^2 = 0.60$  for  $\delta^2\text{H}$ .

**Table 1** Spring data

Spring ID	Latitude	Longitude	Spring elevation (masl)	Measured TDS (mg/L)	Field estimated Q (m <sup>3</sup> /s)	Measured δ <sup>18</sup> O (‰)	Predicted δ <sup>18</sup> O (‰)	Measured δ <sup>2</sup> H (‰)	Predicted δ <sup>2</sup> H (‰)	Spring type <sup>a</sup>
1	37.9588247	-109.8845967	1,915	331	1.49E-06	-12.24	-13.1	-91.3	-96	Extended
2	37.9556301	-109.8722882	1,920	357		-10.72	-13.1	-77.5	-96	Depression
3	37.9539904	-109.8588551	1,949	369		-11.46	-13.2	-84.5	-97	Depression
4	37.9436216	-109.848388	2,011	184		-11.98	-13.3	-90.1	-98	Contact
5	37.9484794	-109.8913571	1,900	796		-11.57	-13.1	-87.9	-96	Depression
6	37.9487129	-109.8947742	1,892	1552		-10.80	-13.1	-81.9	-96	Depression
7	37.9546144	-109.9018294	1,893	387		-12.15	-13.1	-90.5	-96	Extended
9	37.9613708	-109.961232	1,860	409		-12.53	-13	-93.6	-96	Contact
17	37.8381204	-109.7941302	2,647	224		-14.88	-14.5	-108.2	-106	Extended
18	37.8816805	-109.814505	2,607	188	6.51E-05	-14.58	-14.4	-106.2	-106	Extended
19	37.8450582	-109.8512605	2,608	211		-14.53	-14.4	-107.2	-106	Extended
20	37.8670582	-109.9281351	2,348	252	2.15E-07	-13.97	-13.9	-104.6	-102	Contact
21	37.8724154	-109.9727673	2,196	301	1.56E-06	-13.78	-13.6	-103.6	-100	Extended
22	37.9107135	-109.9813603	1,965	250	2.50E-04	-13.80	-13.2	-103.7	-97	Contact?
24	37.8973312	-109.9444182	2,228	284	1.17E-06	-13.89	-13.7	-104.8	-101	Extended
25	37.9182044	-109.9451301	2,178	225	1.56E-05	-13.54	-13.6	-102.1	-100	Extended
27	37.9868942	-109.8991628	1,956	272	6.94E-08	-13.24	-13.2	-100.8	-97	Contact
32	37.9621048	-109.9608566	1,823	402	1.25E-04	-12.01	-13	-92.0	-95	Contact
33	37.9691299	-109.9466684	1,822	427		-11.51	-13	-86.4	-95	Depression
35	37.970512	-109.9559126	1,816	430	1.78E-04	-11.18	-12.9	-85.0	-95	Contact
36	37.9435533	-109.9483477	1,859	324		-11.99	-13	-92.9	-96	Contact
38	37.9666145	-109.8569704	2,030	230	7.18E-08	-11.95	-13.3	-89.5	-98	Contact

<sup>a</sup> See 'Hydrology' section for explanation of spring types

Precipitation and deep groundwater samples are necessary in order to fully constrain the sources of water in springs; however, no groundwater wells exist in Gypsum Canyon watershed, and a rain sample was unattainable. Instead, the stable isotopic ratios of spring water samples are compared to the predicted isotopic ratios of precipitation from the Online Isotopes in Precipitation Calculator (OIPC; Bowen 2003, 2012) in order to partially constrain the origin of water in the spring. The OIPC uses latitude, longitude, and elevation data combined with a model based on the empirical relationship of the GMWL to predict stable isotope ratios in precipitation around the world.

The comparisons reveal that springs at high elevation, greater than ~2,100 masl, have measured isotopic ratios that are similar or slightly lighter than predicted precipitation isotopic ratios. It is assumed that springs with isotopic ratios similar to predicted are primarily composed of recent meteoric water that infiltrated quickly and flowed in the shallow subsurface to its discharge point. Most of the high-elevation spring samples lie within the margin of error of their predicted isotopic value, indicating that the water in them is primarily meteoric water.

Most low elevation springs, however, have measured isotopic values that are heavier than predicted (Fig. 5). There are two low-elevation spring samples that are not heavier than predicted. The lower slope of the line formed by the measured data (Fig. 5c) as compared to the GMWL suggests that evaporation may have occurred between precipitation and sampling, but it is difficult to know when this evaporation happened. Since most recharge in the aquifer likely occurs in wetter, higher elevations, one explanation for heavier isotopic ratios at low elevations is that evaporation occurs before water infiltrates at high elevations, which seems somewhat unlikely given that water discharging at high elevations does not show evidence of evaporation. A second explanation is that water recharged at high elevations mixes with deeper water, possibly from the Lower Cutler or Honaker Trail formation, with heavier isotopic ratios as it travels to its discharge point at lower elevations. The isotopic evidence also suggests that infiltration at low elevations is possible, given that two low-elevation spring-water samples have isotopic ratios nearly identical to what is predicted at that location and elevation.

The exact processes at work in the springs are difficult to know with certainty without further isotopic analysis of precipitation and deep groundwater in this region, but the data presented are valuable in constructing a groundwater flow model. The isotopic data show that most recharge occurs at elevations above 2,100 masl, and recharge is possible at low elevations, though less prevalent. It is likely that most low elevation springs contain meteoric water that has mixed with deeper water in the aquifer.

**Total dissolved solids analysis**

The concentration of total dissolved solid (TDS) in water samples is a proxy for salt content. The concentration of

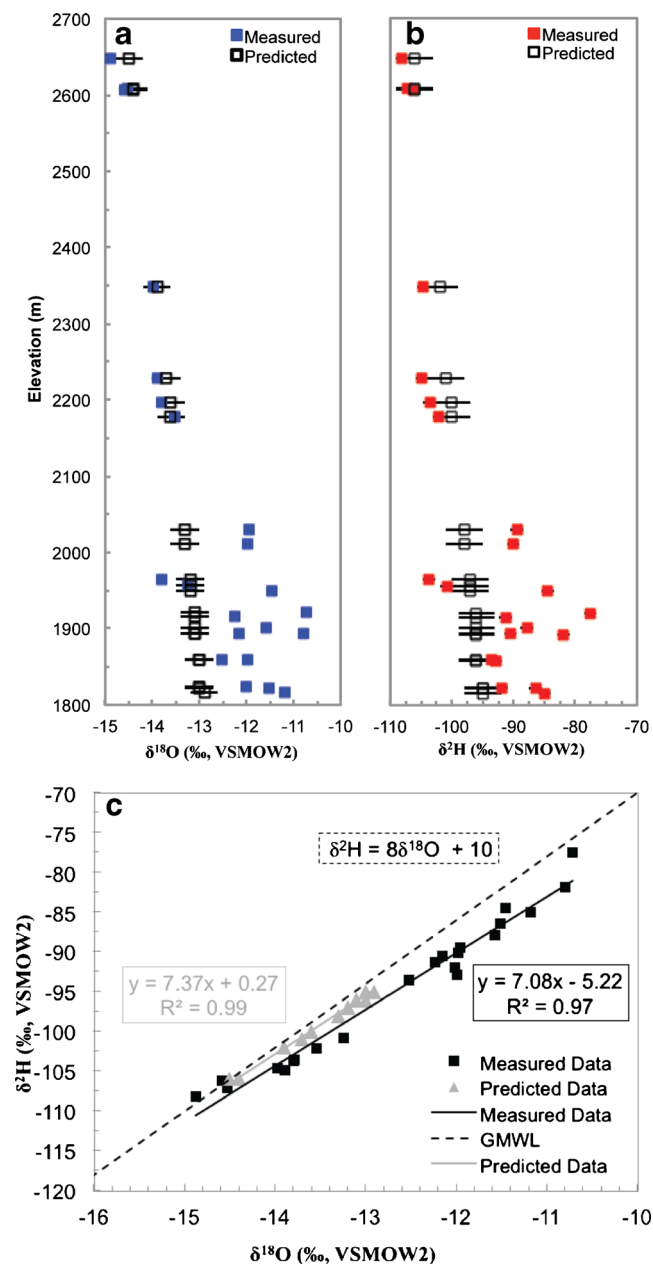


**Fig. 5** Measured and predicted stable isotope ratios from spring samples are shown for **a**  $\delta^{18}\text{O}$  and **b**  $\delta^2\text{H}$  compared to the elevation of the spring. Bars show range of uncertainty. **c** Measured and predicted stable isotope ratios of spring samples compared to the GMWL

TDS in spring water samples was measured using a Hach Conductivity and TDS meter and ranges from 184 to 1,552 mg/L (Table 1; Figs. 6 and 7) with a mean of 382 mg/L, a median of 312.5 mg/L, and a standard deviation of 292.3 mg/L. Most samples are between 210 to 430 mg/L, with two samples above 430 mg/L and one sample below 210 mg/L.

TDS concentration of all samples measured in 2012 shows a weak correlation to elevation with the relationship having an  $R^2$  value of 0.14. The two samples measured in 2012 with the highest TDS were taken in Beef Basin, a local topographic depression. It is probable that the

residence time of groundwater is longer in Beef Basin, leading to locally increased TDS concentrations because the groundwater would have had more opportunity to mix with deeper groundwater with higher TDS. If these two outliers are removed from the dataset, the relationship between elevation and TDS concentration strengthens, with  $R^2=0.53$  for 2012 samples (Fig. 7).

The concentration of TDS in water samples that are isotopically similar to precipitation is between 184–301 mg/L. Thus, it is assumed that TDS concentration of precipitation in the study area is less than  $\sim 200$  mg/L. The National Atmospheric Deposition Program (National Atmospheric Deposition 2007) measures chemistry of precipitation at 257 sites across the country. The nearest site is in the Island in the Sky portion of Canyonlands National Park,  $\sim 50$  km north of the study area. It has records since 1997 and is at 1,797 masl. The 1997–2011 average TDS concentration of precipitation measured at Island in the Sky is 4.4 mg/L, and the average maximum is 25.39 mg/L. This suggests that even the high elevation spring samples that are isotopically similar to precipitation are shallow groundwater, and likely gain TDS as they flow through the aquifer, which also indicates that the TDS concentrations recorded throughout the watershed are not necessarily the sole product of mixing with deep water with high TDS from an evaporite layer. Water may also gain TDS as it travels through the aquifer. Although more chemical analyses are needed in order to differentiate between these two sources of TDS, the TDS data collected in 2012 are useful for constructing and calibrating a model, as the data clearly show an increase in TDS concentration with a decrease in elevation.

### Hydraulic conductivity

Permeameter tests were conducted on samples from the three most commonly observed rock types in order to determine the minimum bound of matrix hydraulic conductivity of representative units since existing hydraulic conductivity data are nonexistent in the studied watershed. Hand samples of tan coarse sandstone, red fine sandstone, and limestone were collected, and hydraulic conductivity was measured using a constant head Trautwein M100000 Standard Panel permeameter. Data are presented in Fig. 2.

The permeameter tests measured six orders of magnitude of variation ( $10^{-11}$  to  $2.6 \times 10^{-5}$  m/s) in hydraulic conductivity of rocks in the study area, often between layers in the same geologic unit, indicating high heterogeneity throughout the studied watershed. Field observations, permeameter data, and the well-known relationship between hydraulic conductivity and volume of rock tested (Schulze-Makuch et al. 1999), with small-volume measurements (e.g. permeameter tests) resulting in much lower hydraulic conductivity than large-volume measurements (e.g. pumping tests), indicate that aquifers in the study region likely have much higher hydraulic conductivity than measured in hand samples. Results of permeameter tests combined with field observations

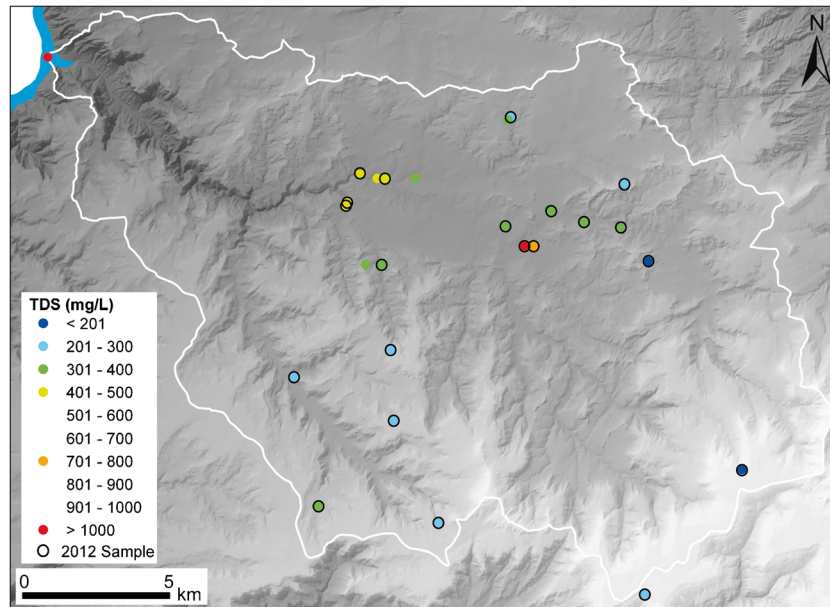


Fig. 6 TDS concentrations measured in spring water samples. 2012 and historical samples are shown

suggest that fracture permeability and flow along bedding planes are first-order controls on groundwater flow. Measured hydraulic conductivity provided a lower bound during parameterization of the groundwater flow model, but measured values were scaled up substantially in the final model in order to reflect the dominance of secondary permeability.

**Groundwater flow and transport modeling**

The objective of groundwater flow modeling is to gain an understanding of the groundwater flow system in the absence of wells and to help constrain and elucidate

groundwater’s contribution to subsurface evaporite dissolution. Modeling TDS transport is used to investigate the transport system and constrain how much dissolution might be occurring in the study region. Together, modeling allows investigation of the dynamics in the groundwater flow and transport systems.

The model is parameterized and constrained using the aforementioned data. Conceptually, water is recharged in and flows from high topography in the southeast towards the Colorado River in the northwest. Discharge occurs at many springs and washes in the watershed and at the mouth of Gypsum Canyon into the Colorado River. TDS is assumed to originate with a subsurface evaporite layer and travel up into the watershed via advection and dispersion. A three-dimensional (3D) model is used to better reproduce the complex topography and heterogeneity of the watershed. TDS, stable isotope, and PRISM precipitation data and the geology and surface topography of the region are used to construct the model. Model outputs include distributions of hydraulic head, flow velocity, TDS concentration, and water and solute budgets. Calibration was used to find appropriate parameter values, and sensitivity analysis was used to investigate parameter uncertainty. Dissolution is calculated from model output.

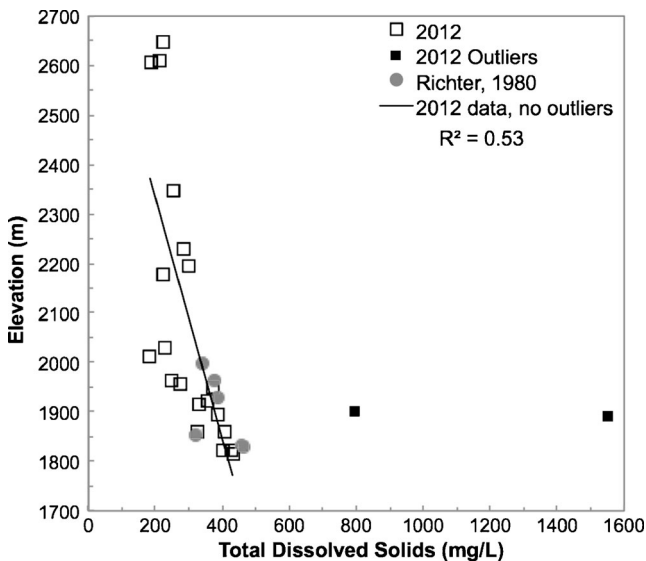


Fig. 7 Relationship between elevation and TDS concentration in spring water. Lower elevation springs have higher TDS concentrations. 2012 samples, including two outliers, and historical data from Richter (1980) are shown

**Numerical model and governing equations**

The US Geological Survey SUTRA code (Voss and Provost 2010) and the ArugsONE graphical interface (Voss et al. 2001) were used to construct the model. SUTRA is a finite-element numerical model for simulating 3D groundwater flow and solute transport. The model is based on mass-balance equations governing groundwater flow and solute transport. The physical processes that govern solute transport are advection, hydrodynamic

dispersion, and retardation. This model assumes that TDS acts as a conservative solute, and no retardation or production of the solute within the aquifer occurs.

**Model setup and boundary conditions**

The model domain encompasses the Gypsum Canyon watershed covering an area of approximately 310 km<sup>2</sup>. The vertical extent includes four conductivity zones representing the geologic units (Fig. 8). The model domain is discretized into 16 vertical layers of equal thickness, with total thickness varying from 128 to 1,834 m. Element thickness varies from approximately 10 to 110 m. Size of the elements in the gridded mesh varies spatially and is ~86 × 86 m on average. There are

41,806 elements and 43,189 nodes in each layer. The model top ranges in elevation from ~2,830 masl on the southeast side, representing the height of the high topography, to ~1,100 masl on the northwest side, representing the height of the Colorado River. The bottom of the model is at 1,000 masl.

Boundary conditions for groundwater flow (Fig. 8a) are assigned based on the hydrologic conditions of the physical system. No-flow boundaries are assumed for the bottom, representing low-permeability evaporite deposits of the Paradox Formation, and on all non-river sides, representing the water divides that define the watershed boundary. The Colorado River boundary in the northwest is specified hydraulic head with head ~25 m below the elevation of the river surface. The model top has recharge

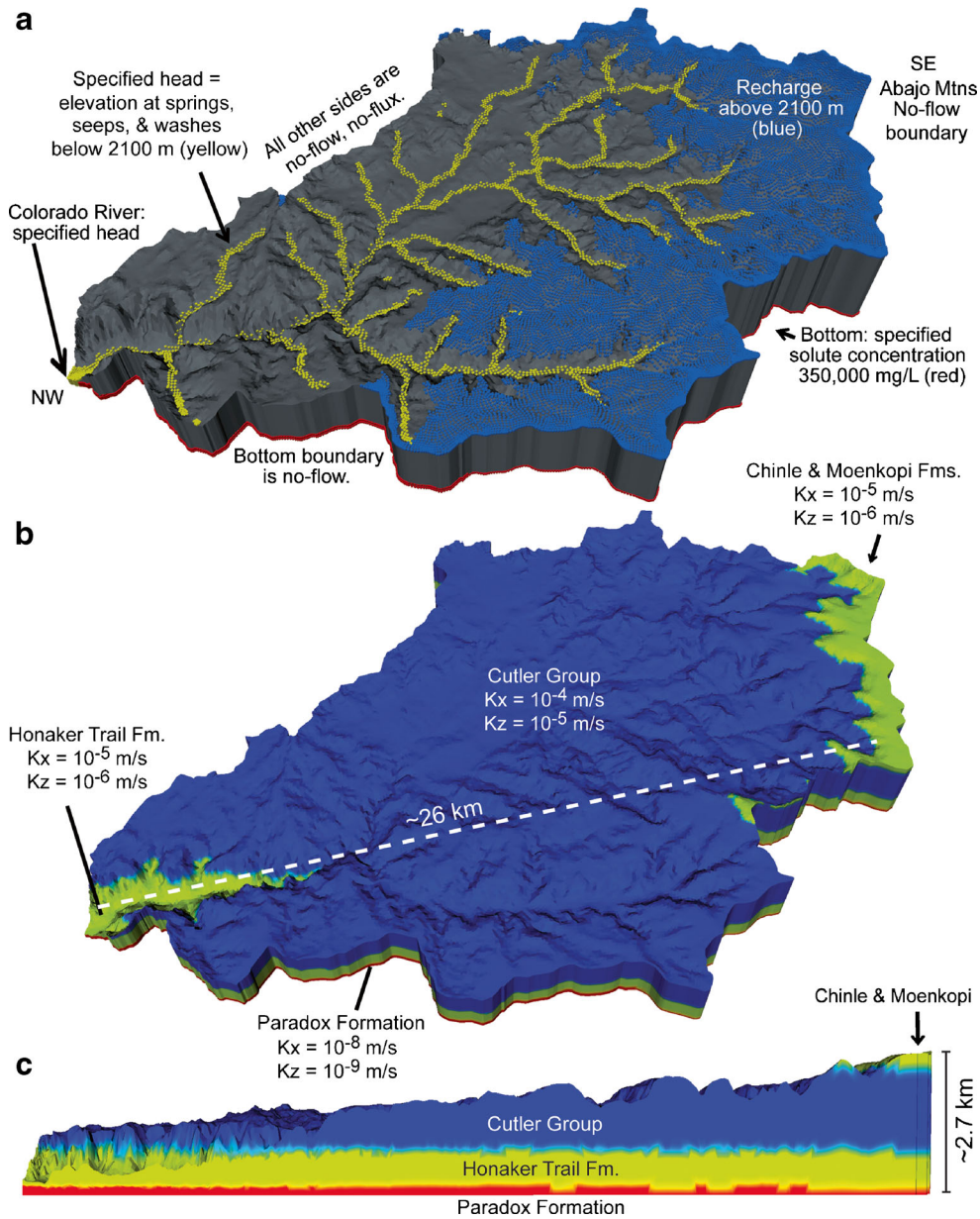


**Fig. 8** Model domain and input parameters. **a** Model boundary conditions. **b** Hydraulic conductivity parameterization. *Dashed line* is location of cross section in part **c**. **c** Hydraulic conductivity zones in cross section. Vertical exaggeration is 2.5 times

above 2,100 masl (Fig. 8a), where stable isotope data suggest recharge primarily occurs. Below 2,100 masl, hydraulic head is specified equal to elevation of the ground surface at all springs, seeps, washes, and streams, places where the water table intersects with the land surface. The model is run under saturated, steady state conditions in order to approximate the long-term state of the watershed.

The principal solute transport boundary condition is on the bottom of the model (Fig. 8a). The bottom layer is the main TDS source with specified concentration equal to 350,000 mg/L, a representative TDS that closely approximates the solubility of halite in water. Halite is the primary evaporite constituent of the Paradox Formation. TDS that originates in the bottom layer is assumed to be dissolving from an evaporite deposit below the model. Concentration of water entering the model as recharge is 200 mg/L, a constraint derived from measured TDS concentrations of the springs determined to be primarily meteoric water using stable isotope ratio comparisons. All no-flow boundaries defined in the flow solution are no-flux boundaries for the concentration solution. The concentration solution is run under steady-state conditions.

### **Model calibration and input parameters**

Model calibration was conducted to determine the best values for model input parameters. During calibration, model results were compared to measured and estimated data and model input parameters were adjusted to achieve the best match between model output and existing data. The main model input parameter adjusted during calibration was hydraulic conductivity. Spring discharge and TDS concentration were used as calibration criteria. An initial calibration was performed to determine the order of magnitude of hydraulic conductivity, using inputs ranging from  $10^{-9}$  to  $10^{-2}$  m/s and permeameter data as a minimum bound. Hydraulic conductivity in the model is spatially distributed based on hydrogeologic units (Figs. 2 and 8). Hydraulic conductivity in the model is one order of magnitude greater in the horizontal direction than in the vertical direction to reflect vertical anisotropy that results from the secondary permeability of the system. Hydraulic conductivity is scaled up from permeameter data to reflect secondary permeability. Dispersivity is 20 m in all directions.

The TDS concentration on the bottom boundary, 350,000 mg/L, was selected to approximate the solubility of halite in water, and hydraulic conductivity was varied until concentration on the surface of the model was the same order of magnitude as measured TDS.

PRISM precipitation data (PRISM Climate Group at Oregon State University 2013) and modeled water budget were used to constrain recharge. Only a small percentage of precipitation is expected to become recharge to the groundwater system because of high evapotranspiration rates (Scanlon et al. 2006), but no data are available to constrain the recharge rate in the studied watershed. In the high-elevation forested area of the watershed, 10–15 % of precipitation probably infiltrates, whereas at low desert

elevations, infiltration is probably closer to 0–5 %. The model assumes that 10 % of precipitation provided by the PRISM model for elevations above 2,100 masl infiltrates as recharge. Hydraulic conductivity was varied until the order of magnitude of modeled spring discharge matched the order of magnitude for the average of estimated spring discharges.

In the horizontal direction, calibration results in the model having a hydraulic conductivity of  $10^{-5}$  m/s where the Chinle and Moenkopi Formations outcrop, above 2,450 masl, (Fig. 8b,c),  $10^{-4}$  m/s where the Cutler Group exists, between 2,450 and 1,600 masl, and  $10^{-5}$  m/s where the Honaker Trail and exposed Paradox Formations exists, below 1,600 masl. Horizontal hydraulic conductivity of the bottom layer of the model is  $10^{-8}$  m/s, representing the unexposed, low permeability Paradox Formation evaporites and shales. The calibrated model based on 10 % infiltration is called the “base model” hereafter. Alternative model runs were conducted for 5 and 15 % infiltration.

During calibration, results of model runs were compared to field data that were not used as input parameters in order to calibrate and check the model outputs. Measured TDS and estimated spring discharge were compared to modeled TDS and discharge using the model node(s) closest to the spring to approximate the spring’s location (Fig. 9). After calibration, modeled TDS shows the same pattern as measured TDS, but is generally lower than measured TDS and does not capture the full range of variability (Fig. 9a). Similarly, modeled spring discharge does not capture the full range of variability in estimated spring discharge (Fig. 9b), but the average of discharge at springs from the base model,  $3.2 \times 10^{-5}$  m<sup>3</sup>/s, is similar to the average of estimated discharge,  $5.7 \times 10^{-5}$  m<sup>3</sup>/s. Calibration was ended when a parameter set was attained that creates a model producing TDS concentrations and spring discharges that are the same order of magnitude and a similar pattern to field data.

### **Model results for groundwater flow**

Model output shows hydraulic heads that are higher in the southeast and lower in the northwest, driving groundwater flow generally from the southeast to northwest, towards the Colorado River (Fig. 10). There are many near-surface local flow systems driven by steep local topographic and head gradients (Fig. 10a). Water flows towards topographic depressions such as Fable Valley, Beef Basin, Gypsum Canyon, and the Colorado River. The average hydraulic head gradient over the entire domain is approximately 150 m/km. Groundwater velocity in the base model varies from approximately  $10^{-12}$  to  $10^{-3}$  m/s. The amount of water that enters the system through the top recharge boundary above 2,100 masl is  $7.5 \times 10^6$  m<sup>3</sup>/year for the base model. Water exits the model through springs, seeps, and washes below 2,100 masl and at the mouth of Gypsum Canyon into the Colorado River.

### **Model results for solute transport**

Solute concentration increases with depth into the model, and is highest at the bottom of the model, near the

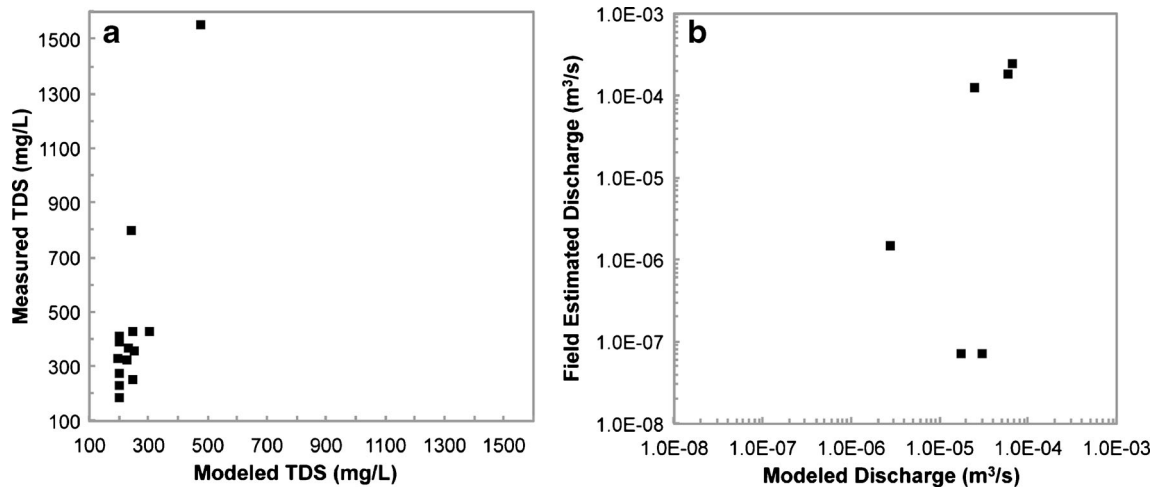


**Fig. 9** Comparison of observed and modeled data. **a** Modeled and measured TDS concentration. The pattern of concentration is similar, but variations in magnitude exist. **b** Modeled and estimated spring discharge. Estimated discharge is more variable than modeled discharge, but the average of modeled discharge is similar to the average of estimated discharge

specified concentration layer (Fig. 11). The amount of solute that enters the system through the bottom specified concentration boundary is  $7.2 \times 10^3$  mg/s. The amount of solute that enters the model via recharge is  $4.8 \times 10^4$  mg/s, and the amount of solute that discharges from the model on the top surface and at the Colorado River is  $6.2 \times 10^4$  mg/s. On the surface, solute concentration is highest in the bottom of Gypsum Canyon and generally higher in valleys, washes, and basins than in the surrounding areas (Fig. 11b). Figure 11b shows modeled concentrations ranging from ~225 to ~500 mg/L in most of the valleys. The modeled concentrations are ~500–5,000 mg/L in some places in Gypsum Canyon. Local flow paths appear to exert a strong control on solute concentration, an indication that advection is the primary mode of solute transport.

Modeled TDS concentration on the surface is similar to the pattern of TDS values measured in springs in 2012 (Fig. 9) and the measurements from historical records (Richter 1980; UGS 1948 accessed via Utah Geological Survey 2012), but the model does not replicate the magnitude of variability. Modeled TDS concentration overestimates the one historical observed concentration in Gypsum Canyon, but underestimates observed concentrations in most of the measured springs (Figs. 9 and 11b).

**Sensitivity analysis**

Uncertainties exist in the hydraulic conductivity, bottom solute concentration, and recharge model parameter values, as well as the role that faults play in solute transport and salt dissolution. Sensitivity analyses were

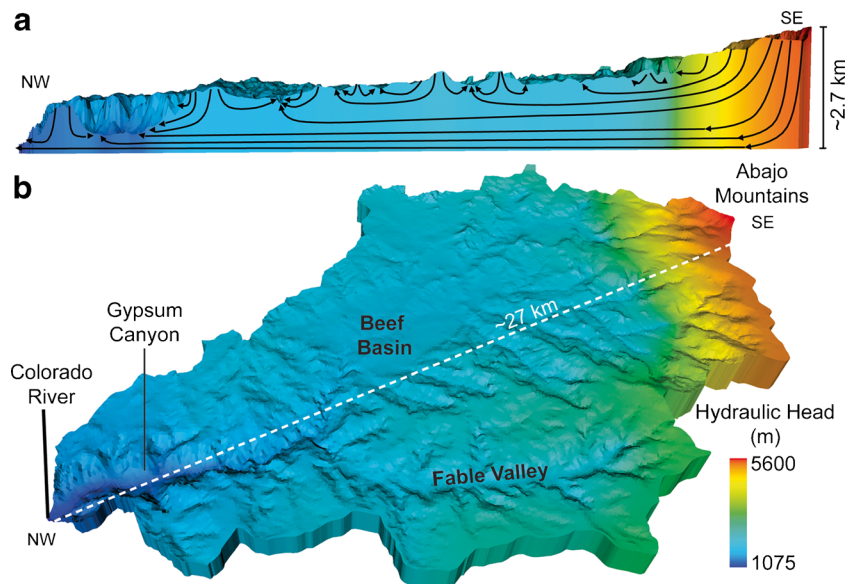


**Fig. 10** Modeled hydraulic head and groundwater flow paths. **a** Cross-section view of the watershed with regional and local flow systems. Flow lines, in black, are drawn on the basis of flow vectors and hydraulic head (rainbow colors). Vertical exaggeration is 2.5 times. **b** Oblique view of the watershed showing hydraulic head. Dashed line is location of cross section in part a

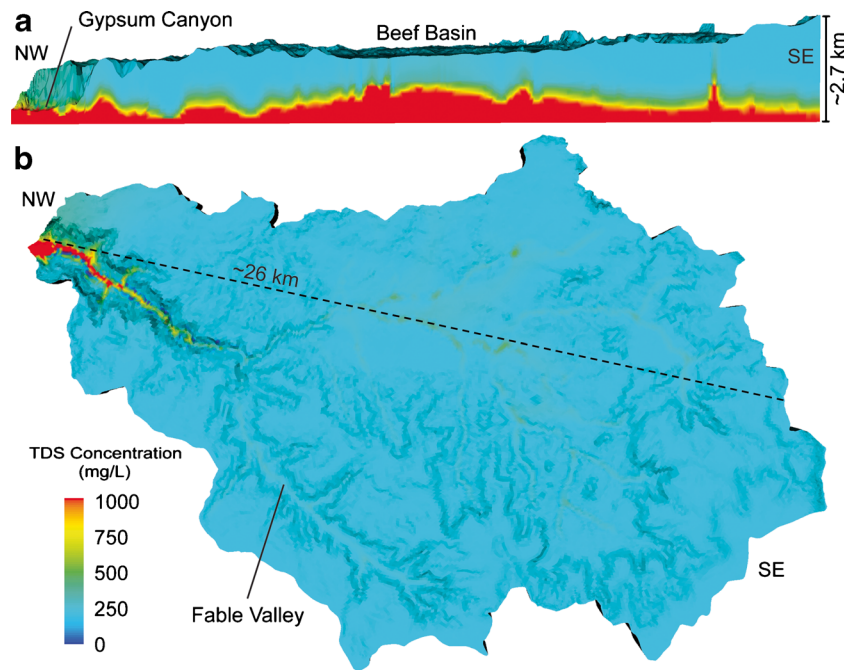


**Fig. 11** Modeled TDS concentration. TDS concentration is shown with a scale cropped at 1,000 mg/L in order to see the small differences in the valleys. The model captures the general pattern of measured TDS, but does not reproduce the full range of variability. **a** Cross section through Gypsum Canyon and Beef Basin. This is a different cross section than Fig. 10. Vertical exaggeration is 2.5 times. **b** Surface TDS concentration. *Dashed line* is location of cross section in part **a**

conducted to examine these uncertainties, and the results are presented in Table 2. Hydraulic conductivity was varied by one order of magnitude higher and lower than the values used in the base model. Changing hydraulic conductivity has a small effect on solute concentration, likely due to the steady-state condition, and a larger effect on flow velocity and hydraulic head (Table 2). Similarly, alternative model runs with 5 and 15 % infiltration mostly affect hydraulic head and flow velocity (Table 2).

The bottom concentration parameter was varied by one order of magnitude lower. Since the concentration closely approximates solubility of halite in water, it is unrealistic to increase it. TDS concentration is very sensitive to changes in bottom TDS concentration. The low bottom concentration case results in surface concentrations that are too low overall as compared to field data. Since the base model overestimates surface concentration in Gypsum Canyon, but underestimates TDS concentration at most springs, the base model bottom solute concentration value of 350,000 mg/L remains a better estimate of the parameter than the low case.

There are numerous faults near the study area (Fig. 1), but no data on fault hydraulic conductivity is available. A version of the base model was constructed that incorporates large faults as high conductivity conduits because they are active normal faults. Hydraulic conductivity in faults is  $10^{-3}$  m/s throughout the upper model where faults exist on the surface, a value chosen because it is one to two orders of magnitude greater than hydraulic conductivity of the most conductive geologic unit. Faults in the region do not extend into the Paradox Formation (Huntoon 1986). The pattern of surficial concentration does not change significantly when

faults are incorporated into the model. TDS concentrations in Gypsum Canyon and the washes and valleys remain similar to their values in the base model. Water velocity, however, is increased in the faults, and small changes in TDS concentration were observed near the faults at depth. Thus, faults may alter concentrations of TDS locally, but have little effect on the system as a whole.

Results of the sensitivity analysis indicate that the base model input parameters likely capture the correct order of magnitude for the specified parameters as compared to the actual system. Fine-tuning parameters within the specified order of magnitude may result in slightly improved models. The current model represents the overall patterns of flow and transport seen in the field, but not all the variability. It is a reasonable first step in describing the general groundwater flow and solute transport patterns of the system.

### Evaporite dissolution

The modeled solute budget and concentration distribution were used to estimate evaporite dissolution rate, assuming that solute inflow from the bottom layer of the model is equal to the amount of dissolution that occurs in the evaporite below. Model output gives a flux of solute through each node in mass per time. An estimate of salt dissolution on the bottom of the model domain was made using solute inflow on the bottom layer of the base model, 7152 mg/s, and the density of halite, 2168 mg/cm<sup>3</sup>, resulting in a mass of 225,710 kg or a volume of 104 m<sup>3</sup> of salt dissolving from the bottom of the model in one year. This amount of dissolution divided by the area of the

**Table 2** Sensitivity analysis data

Parameter specifications:	Base case	Low K	High K	Low C	5 % recharge	15 % recharge
Hydraulic conductivity (m/s)	Chinle and Moenkopi (Kx, Kz) IE-05, IE-06 Cutler Group (Kx, Kz) IE-04, IE-05 Honaker Trail (Kx, Kz) IE-05, IE-06 Paradox (Kx, Kz) IE-07, IE-08 On bottom 350,000 In recharge 200 % PRISM Precip. 10 %	IE-06, IE-07 IE-05, IE-06 IE-06, IE-07 IE-09, IE-10 350,000 200 10 %	IE-04, IE-05 IE-03, IE-04 IE-04, IE-05 IE-07, IE-08 350,000 200 10 %	IE-05, IE-06 IE-04, IE-05 IE-05, IE-06 IE-08, IE-09 35,000 200 10 %	IE-05, IE-06 IE-04, IE-05 IE-05, IE-06 IE-08, IE-09 350,000 200 5 %	IE-05, IE-06 IE-04, IE-05 IE-05, IE-06 IE-08, IE-09 350,000 200 15 %
Recharge						
Results:						
Hydraulic head (masl)	5,560 1,075 1,41E-03 2,00E-12 ~500-5,000 ~225-500	2,428 1,075 6,44E-03 6,54E-12 ~500-5,000 ~225-400	37,299 1,075 1,45E-03 1,75E-13 ~500-5,000 ~225-700	5,560 1,075 1,41E-03 2,00E-12 ~225-1,200 ~200-225	3,834 1,075 6,91E-04 1,00E-12 ~500-5,000 ~225-500	7,366 1,075 2,13E-03 1,00E-12 ~500-5,000 ~225-500
Water Velocity (m/s)	Maximum 1,075 Minimum 2,00E-12	239,06 308,02	239,06 1,88 -240,93	239,06 26,65 -265,71	119,53 29,96	358,58 24,91
Surface solute concentration (mg/L)	Gypsum Canyon Valleys Everywhere else In as recharge In at specified head Out at specified head	~500-5,000 ~225-500 ~200 239,06 308,02	~500-5,000 ~225-700 ~200 239,06 1,88 -240,93	~500-5,000 ~225-1,200 ~200-225 239,06 26,65 -265,71	~500-5,000 ~225-500 ~200 119,53 29,96	~500-5,000 ~225-500 ~200 358,58 24,91
Water flow (L/s)						
Estimated dissolution (per year)	TDS Inflow on bottom (mg/s) 7,152,48 Weight (kg) 2,26E+05 Volume (m <sup>3</sup> ) 104,11 mm <sup>3</sup> 3,36E-04	23,758,90 7,50E+05 345,83 1,12E-03	5,536,47 1,75E+05 80,59 2,60E-04	711,52 2,25E+04 10,36 3,34E-05	4,566,03 1,44E+05 66,46 2,14E-04	9,749,39 3,08E+05 141,91 4,58E-04

<sup>a</sup> See 'Evaporite dissolution' section for explanation of how this is calculated

model domain is equal to  $\sim 3.4 \times 10^{-4}$  mm/year. In order to account for uncertainty in input parameters, dissolution calculations were repeated for the high and low hydraulic conductivity cases, the low bottom concentration case, and the 5 and 15 % infiltration cases. These calculations result in a range of dissolution values from  $3.4 \times 10^{-5}$  to  $1.1 \times 10^{-3}$  mm/year (Table 2). In order to investigate local variability, dissolution was also calculated for the nodes with the least and most solute inflow, resulting in local dissolution values spanning ten orders of magnitude.

**Discussion**

**Discussion of model results with observed data**

The general groundwater flow and TDS concentration patterns from this model are consistent with field observation and previous studies (Huntoon 1979; Paiz and Thackston 1987a, b; Richter 1980), although the model does not capture all the variability of field measurements. Measured and modeled data show that TDS concentrations increase with depth into the aquifer and laterally increase towards the discharge locations. The model simulated the pattern of measured TDS concentration of shallow groundwater samples (Figs. 6 and 11), indicating that a deep evaporite layer and mixing within the aquifer can create the TDS pattern observed on the surface. However, this result can only be confirmed by further water chemistry analysis of the sampled spring water in order to constrain the sources of TDS.

The model results corroborate previous studies that reported water quality in the greater Canyonlands area generally deteriorates with depth and is highly variable, with springs ranging from fresh to saline (Bishop 1996; Richter 1980). No wells, and therefore no isotopic or salinity data on deep groundwater exist within Gypsum Canyon watershed. Of the spring samples measured, the low elevation springs have enriched isotopic signatures and higher TDS concentrations. If it is assumed that most recharge occurs in the higher elevations, then the most likely explanation for enriched isotopic signatures of the low elevation spring samples is that some deeper water within the aquifer has enriched isotopic signatures and mixes with the meteoric water recharged at high elevations. It is also possible that the heavier isotopic ratios are a result of evaporation; however, the TDS data presented, combined with the modeled flow paths, suggest that that shallow and deep water within the aquifer can mix, and may account for both heavier isotope ratios and increased TDS concentrations at lower elevations. Furthermore, these results agree with Nuckolls and McCulley (1987) who analyzed stable isotopes in Honaker Trail spring samples north of the study region and found that spring water is mostly meteoric water with a small component of saline groundwater.

The difference between measured and modeled hydraulic conductivity provides a basis for previous conjecture (Richter 1980) and field observations that fracture permeability is a primary control on groundwater flow in

the watershed. The low hydraulic conductivities measured in rock samples as compared to higher hydraulic conductivity used in the model, and field observations, indicate that groundwater flow is primarily through fractures.

The modeling results presented here offer, for the first time, a description of the groundwater flow and solute transport systems in Gypsum Canyon watershed and how individual parameters affect the system as a whole. The model can subsequently be used to estimate information that cannot be directly measured in the field such as subsurface dissolution.

### **Implications for Paradox evaporite dissolution and associated fault slip**

On average, the amount of dissolution occurring in the evaporite deposits underlying the watershed as indicated by the model is not enough to account for the change in volume associated with the observed fault slip rate. InSAR analysis indicates that the fastest moving faults in the region slip at a rate of 1–2 mm/year (Furuya et al. 2007). When subsurface evaporite deposits are dissolved by groundwater, a void can be created between the dissolving layer and the overlying rock burden. If the void becomes large enough, it may cause fault slip or subsidence of the overlying rock. However, this modeling study implies that only  $10^{-5}$ – $10^{-3}$  mm of vertical displacement per year can be attributed to dissolution by groundwater flow. The highly variable rate of solute inflow at model nodes indicates that localized dissolution may be larger than the average and may cause volume loss that could result in fault slip or ground subsidence in local regions. Furthermore, since salt deforms in a ductile manner, flowing rather than fracturing under most geological conditions, groundwater may enhance and increase internal salt flow by hydrologic weakening, driving fault slip without accounting for all of the deformation via volume loss from groundwater-driven dissolution. Fault slip and subsidence may be the result of a combination of processes that include dissolution via groundwater flow, salt flow, and internal deformation within the salt deposits.

### **Limitations**

Very limited data are available in this hard-to-access field site to support complexities in model parameters, so the model structure is simplified in an attempt to capture the general flow and transport patterns. The sensitivity analysis addresses some of this simplification; however, the model presented contains limitations. The groundwater flow and solute transport solutions are run assuming steady-state conditions. This assumption is meant to approximate the long-term hydrologic setting. Some discrepancies between modeled results under the steady-state assumption and measured values may be reduced if a transient model is used. The steady-state model assumes an average precipitation regime, but not a uniform one. A particularly dry or wet period would yield slightly different model results, as demonstrated with the sensitivity analysis. Daily, and to some extent annual, variations are dampened with depth.

Groundwater flow and dissolution would increase during wet periods. A dry period would result in decreased groundwater flow and salt dissolution.

For solute transport, the sources of solute are constant through time and space, the solute is assumed to be conservative, and constant density flow is used. A homogeneous distribution of solute on the bottom of the model is assumed because the available data suggest there are evaporites underlying the entire watershed, but the thickness is uncertain. Given that the model's bottom is at the top of the evaporite layer, approximating a heterogeneous evaporite thickness will not significantly alter the model outcome. The lack of deep salinity data inhibits a precise value for TDS concentration at depth. Saltier water is denser, and density-driven groundwater flow may affect groundwater flow paths since gravity forces cause denser water to flow downward relative to less dense water. Higher concentration at the bottom of the aquifer could lead to more diffusion but restricts advective transport of salt, as does anisotropic hydraulic conductivity, which is incorporated in the model. Prior test model runs in 2D suggested no notable differences in model results with density-dependent flow. Furthermore, fluid density increasing with depth is generally considered a "stable density configuration" that "drives no flow" (Voss and Provost 2010). The sensitivity analysis performed on the concentration boundary condition addresses some aspect of this uncertainty, but further investigation may improve model results.

### **Conclusions**

This study provides the first description of the groundwater flow and solute transport systems of the Gypsum Canyon watershed. The following conclusions are drawn:

- Regional groundwater flow is from southeast to northwest, towards the Colorado River. Local, shallow flow systems are common and spring discharge is variable, ranging from  $10^{-8}$  to  $10^{-4}$  m<sup>3</sup>/s.
- Hydraulic conductivity measured with the permeameter ranges from  $10^{-11}$  to  $10^{-5}$  m/s, illustrating heterogeneity within the study region. The difference in hydraulic conductivity between lab results, field observations, and modeling suggests that fracture permeability is a primary control on groundwater flow paths.
- Lower elevation springs have higher TDS concentrations. Solute transport modeling is able to replicate the general pattern of TDS concentration measured in springs, but not the variability. Modeled concentration is highest in Gypsum Canyon and topographic depressions throughout the watershed.
- Stable isotope data, TDS concentrations, and model output reveal that springs above 2,100 masl discharge shallow groundwater that is primarily composed of meteoric water. Springs below 2,100 masl are most likely a mix of meteoric water and deeper aquifer water.

- Modeling indicates that evaporite dissolution via groundwater flow is small on average, on the order of  $10^{-4}$  mm/year, and probably cannot account for observed surface deformation rates, but highly variable localized dissolution may contribute to displacement.
- Motion on active faults may be a combination of dissolution via groundwater flow and internal salt flow. Although incorporating high conductivity fault conduits into the model does not significantly alter model results, fault conduits may provide pathways for locally increased groundwater flow, salt dissolution, and surface deformation.

**Acknowledgements** This study was supported in part by NSF grant EAR 1119173 and the Colorado Ground Water Association. Thank you to the Stable Isotope Lab at the Institute for Arctic and Alpine Research, University of Colorado Boulder for processing stable isotope samples, Jason Reitman for help in the field, and three reviewers for their comments that greatly improved the manuscript.

## References

- Baars DL (2010) Geology of Canyonlands National Park. In Sprinkel DA, Chidsey TC Jr, Anderson PB (eds) *Geology of Utah's Parks and Monuments*, 3rd edn. Bryce Canyon Nat Hist Assoc and Utah Geol Assoc, Salt Lake City, UT
- Barbeau DL (2003) A flexural model for the Paradox Basin: implications for the tectonics of the Ancestral Rocky Mountains. *Basin Res.* doi:10.1046/j.1365-2117.2003.00194.x
- Benito G, Prez-gonzas A, Gutierrez F, Machado MJ (1998) River response to Quaternary subsidence due to evaporite solution (Gallego River, Ebro Basin, Spain). *Geomorphology* 22:243–263
- Benito G, Gutierrez F, Perez-Gonzalez A, Machado MJ (2000) Geomorphological and sedimentological features in Quaternary fluvial systems affected by solution-induced subsidence (Ebro Basin, NE-Spain). *Geomorphology* 33:209–224
- Bishop CE (1996) Potential for potable ground water on state land near Canyonlands National Park, Utah, Section 16, T. 30 S., R. 20 E., Report of Invest. 230, Utah Geol Surv, Salt Lake City, UT, 25 pp
- Bowen GJ (2003) Interpolating the isotopic composition of modern meteoric precipitation. *Water Resour Res.* doi:10.1029/2003WR002086
- Bowen GJ (2012) The Online Isotopes in Precipitation Calculator, version 2.2. Available via <http://www.waterisotopes.org>. Accessed 21 August 2012
- Bryan K (1919) Classification of springs. *J Geol.* doi:10.1086/622677
- Condon SM (1997) Geology of the Pennsylvanian and Permian Cutler Group and Permian Kaibab Limestone in the Paradox Basin, southeastern Utah and southwestern Colorado. *US Geol Surv Bull* 2000-P
- Craig H (1961) Isotopic variations in meteoric waters. *Science.* doi:10.1126/science.133.3465.1702
- Cudlip L, Berghoff K, Vana-Miller D (1999) Water resources management plan Arches National Park and Canyonlands National Park, Utah. Utah State Univ., Logan, UT, 153 pp
- Dansgaard W (1964) Stable isotopes in precipitation. *Tellus* 16(4):436–468
- Evans DG, Nunn JA, Hanor JS (1991) Mechanisms driving groundwater flow near salt domes. *Geophys Res Lett* 18(5):927–930
- Fetter CW (2001) *Applied hydrogeology*, 4th edn. Prentice-Hall, Upper Saddle River, NJ
- Furuya M, Mueller K, Wahr J (2007) Active salt tectonics in the Needles District, Canyonlands (Utah) as detected by interferometric synthetic aperture radar and point target analysis: 1992–2002. *J Geophys Res.* doi:10.1029/2006JB004302
- Ge H, Jackson MPA (1998) Physical modeling of structures formed by salt withdrawal: implications for deformation caused by salt dissolution. *AAPG Bull* 82(2):228–250
- Guerrero J, Gutierrez F, Lucha P (2004) Paleosubidence and active subsidence due to evaporite dissolution in the Zaragoza area (Huerva River valley, NE Spain): processes, spatial distribution and protection measures for transport routes. *Eng Geol.* doi:10.1016/j.enggeo.2003.10.002
- Gutiérrez F (2004) Origin of the salt valleys in the Canyonlands section of the Colorado Plateau: evaporite-dissolution collapse versus tectonic subsidence. *Geomorphology.* doi:10.1016/S0169-555X(03)00186-7
- Huntoon PW (1979) The occurrence of ground water in the Canyonlands area of Utah, with emphasis on water in the Permian section. 9th Field Conf. Guidebook, Four Corners Geol Soc, Durango, CO, pp 39–46
- Huntoon PW (1986) The incredible tale of Texasgulf well 7 and fracture permeability, Paradox Basin, Utah. *Ground Water* 24(5):643–653
- Huntoon PW, Billingsley GH, Breed WJ (1982) Geological map of Canyonlands National Park and vicinity, Utah. Canyonlands Nat Hist Assoc, Moab, UT, Map scale 1:62,500
- Jackson MPA, Schultz-Ela DD, Hudec MR, Watson IA, Porter ML (1998) Structure and evolution of Upheaval Dome: a pinched-off salt diapir. *Geol Soc Am Bull.* doi:10.1130/0016-7606(1998)110<1547:SAEOUD>2.3.CO;2
- Johnson KS (2005) Subsidence hazards due to evaporite dissolution in the United States. *Environ Geol.* doi:10.1007/s00254-005-1283-5
- Lewis RQ, Campbell RH, Thaden RE, Krummel WJ, Willis GC, Matyjasik B (2011) Geologic map of Elk Ridge and vicinity, San Juan County, Utah. Miscellaneous publication 11-IDM. Utah Geol Surv, Salt Lake City, UT, 13 pp
- Lugo AE, Brown SL, Dodson R, Smith TS, Shugart HH (1999) The Holdridge life zones of the conterminous United States in relation to ecosystem mapping. *J Biogeogr.* doi:10.1046/j.1365-2699.1999.00329.x
- Martin L (2001) Drinking water source protection plan Canyonlands National Park. Natl Park Serv Water Resour Div, Fort Collins, CO, 22 pp
- Masoth TW, Tripp BT (2011) Well database of salt cycles of the Paradox Basin, Utah, Open-File Report 581. Utah Geol Surv, Salt Lake City, UT, 13 pp
- McCleary J (1989) Characterization of the Davis Canyon site, San Juan County, Utah, as a potential repository for the disposal of high level nuclear waste and spent fuel. Utah Geol Assoc, Salt Lake City, UT, pp 209–222
- McCleary JR, Romie JE (1986) Stratigraphic and structural configuration of the Navajo (Jurassic) through Ouray (Mississippian-Devonian) Formations in the vicinity of Davis and Lavender Canyons, southeastern Utah, part 1, BMI/ONWI-5. Office of Nuclear Waste Isolation, US Department of Energy, Washington, DC
- National Atmospheric Deposition Program (2007) NADP Program Office, Illinois State Water Survey. Available via <http://nadp.sws.uiuc.edu/>. Accessed 6 Feb 2013
- Nuccio VF, Condon SM (1996) Burial and thermal history of the Paradox Basin, Utah and Colorado, and petroleum potential of the Middle Pennsylvanian Paradox Formation. *US Geol Surv Bull* 2000-O, 41 pp
- Nuckolls HM, McCulley BL (1987) Origin of saline springs in Cataract Canyon, Utah. 9th Field Conf. Guidebook, Four Corners Geol Soc, Durango, CO, pp 193–199
- Paiz CD, Thackston JW (1987a) Hydrogeologic units in Cataract Canyon and vicinity: Paradox Basin, Utah. 9th Field Conf. Guidebook, Four Corners Geol Soc, Durango, CO p 161–171
- Paiz CD, Thackston JW (1987b) Summary of hydrogeologic data and preliminary potentiometric maps in the vicinity of Davis

- and Lavender Canyons, Paradox Basin, Utah. 9th Field Conf. Guidebook, Four Corners Geol Soc, Durango, CO, pp 173–184
- PRISM Climate Group, Oregon State University (2013) Available via <http://prism.oregonstate.edu>. Accessed 6 Feb 2013
- Ranganathan V, Hanor JS (1988) Density-driven groundwater flow near salt domes. *Chem Geol* 74:173–188
- Richter HR (1980) Ground water resources in the part of Canyonlands National Park east of the Colorado River and contiguous Bureau of Land Management lands, Utah. MSc Thesis, University of Wyoming, USA
- Scanlon BR, Keese KE, Flint AL, Flint LE, Gaye CB, Edmunds WM, Simmers I (2006) Global synthesis of groundwater recharge in semiarid and arid regions. *Hydrol Process*. doi:10.1002/hyp.6335
- Schulze-Makuch D, Carlson DA, Cherkauer DS, Malik P (1999) Scale dependency of hydraulic conductivity in heterogeneous media. *Ground Water* 36(6):904–919
- Sumison CT, Bolke EL (1972) Water resources of part of Canyonlands National Park, southeastern Utah, US Geol Surv Open File Rep 72-363, 75 pp
- Trudgill BD (2002) Structural controls on drainage development in the Canyonlands grabens of southeast Utah. *AAPG Bull* 86(6):1095–1112
- Utah Geological Survey (2012) Spring ID 1381 collected in 1948. In: Utah's geothermal wells and springs. Available via <http://geology.utah.gov/geothermal/interactive/index.html>. Accessed 1 May 2012
- Voss CI, Provost AM (2010) SUTRA: a model for saturated-unsaturated variable-density groundwater flow with solute or energy transport, version 2.2. US Geol Surv Water Resour Invest Rep 02-4231, 291 pp
- Voss CI, Boldt D, Shapiro AM (2001) A graphical-user interface for the U.S. Geological Survey's SUTRA code using Argus ONE. US Geol Surv Open-File Rep 97-421, 106 pp
- Walsh P, Schultz-Ela DD (2003) Mechanics of graben evolution in Canyonlands National Park, Utah. *Geol Soc Am Bull*. doi:10.1130/0016-7606(2003)115<0259
- Woods AJ, Lammers DA, Bryce SA, Omemik JM, Denton RL, Domeier M, Comstock JA (1997) Ecoregions of Utah (color poster with map, descriptive text, summary tables, and photographs). US Geological Survey, Reston, VA